SUPPLEMENTAL TABLES AND FIGURES FOR:

Large protein assemblies formed by multivalent interactions between cadherin23 and harmonin suggest a stable anchorage structure at the tip link of stereocilia

Lin Wu, Lifeng Pan, Chuchu Zhang, and Mingjie Zhang

Supplemental Figures

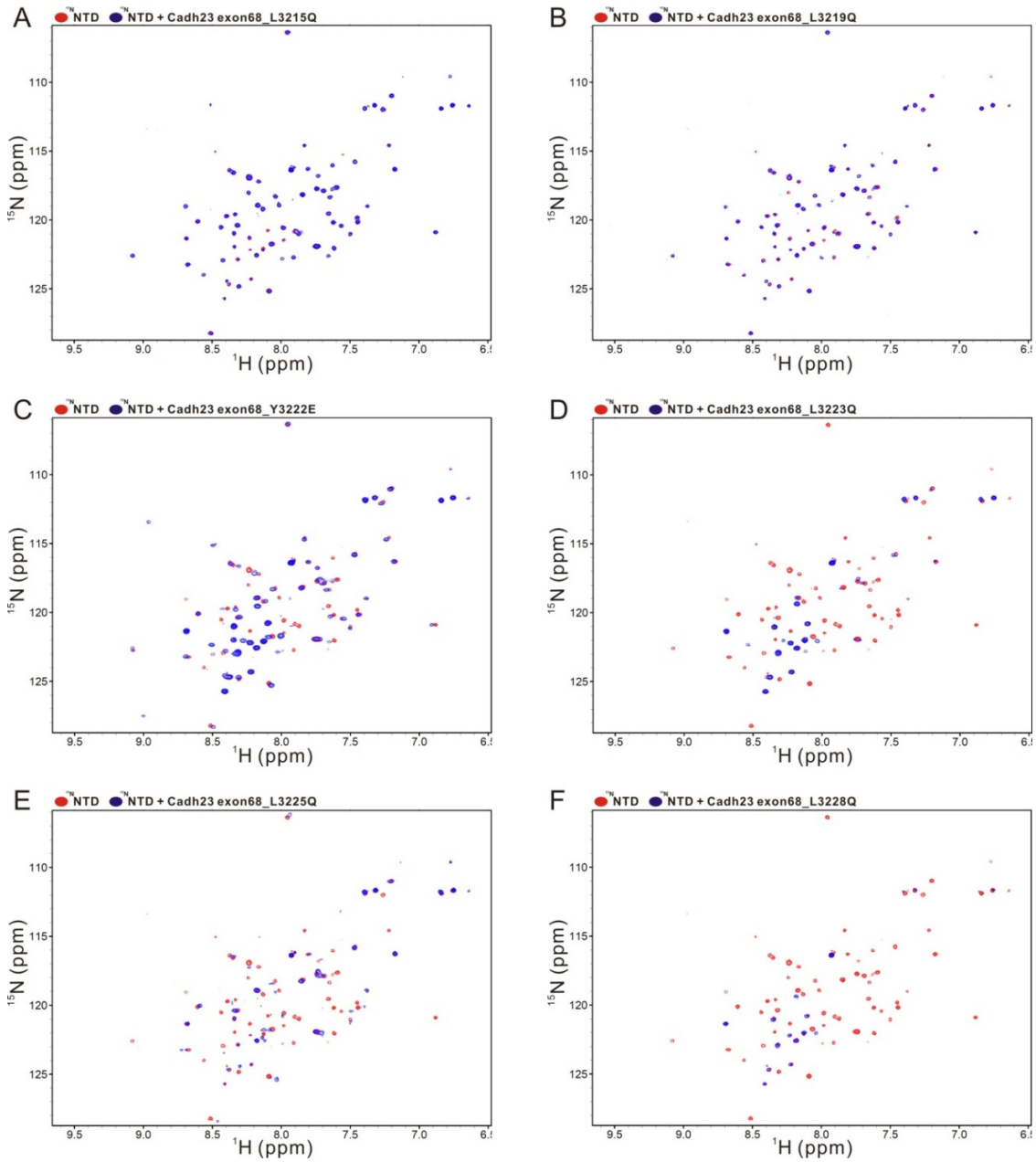

Supplemental Figure S1. Identification of the critical residues of the cadherin23 exon68 peptide required for binding to harmonin NTD. Superposition plot of the ^{1}H-^{15}N HSQC spectra of the free-form harmonin NTD and the protein in the presence of excess amounts of various mutants of GB1-tagged exon68 peptide. *A*-*C*, Substitutions of Leu-3215 (*A*), Leu-3219 (*B*) with Gln, and Tyr-3222 (*C*) with Glu either disrupt or weaken the binding of exon68 peptide to harmonin NTD. *D*-*F*, In contrast, replacement of Leu-3223 (*D*), Leu-3225 (*E*) or Leu-3228 (*F*) with Gln had no obvious impact on the peptide's binding to harmonin NTD.

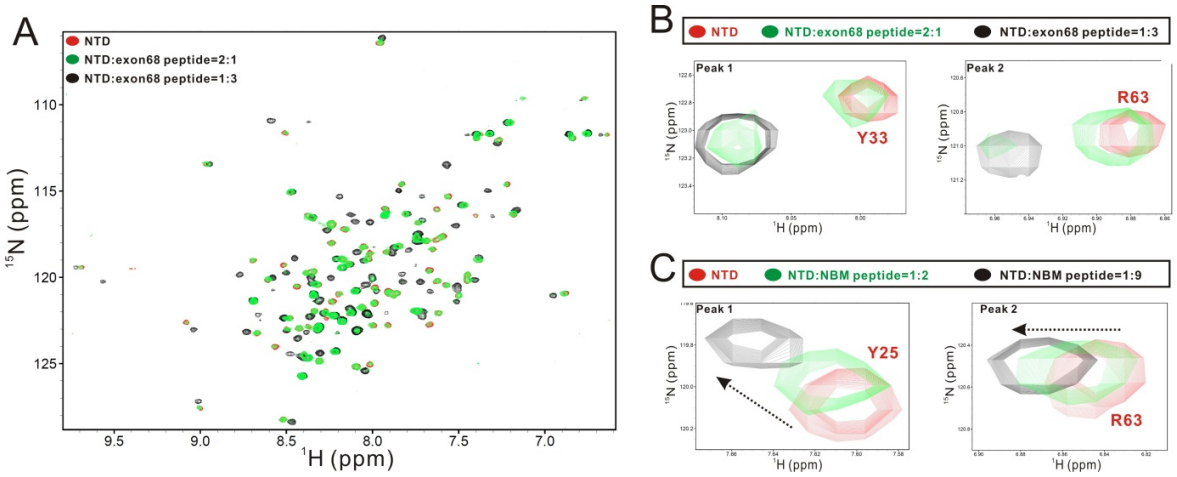

Supplemental Figure S2. The NTD binding affinity of exon68 peptide is stronger than that of NBM peptide. *A*, Superposition plot of the ^{1}H-^{15}N HSQC spectra of harmonin NTD with increasing molar ratios of exon68 peptide. *B*, Overlay plots of two selected Tyr-33 and Arg-63 peaks of NTD ^{1}H-^{15}N HSQC spectra show slow exchange patterns during exon68 peptide titration. *C*, Superposition plots of two selected Tyr-25 and Arg-63 peaks of NTD ^{1}H-^{15}N HSQC spectra show fast exchange patterns during NBM peptide titration.

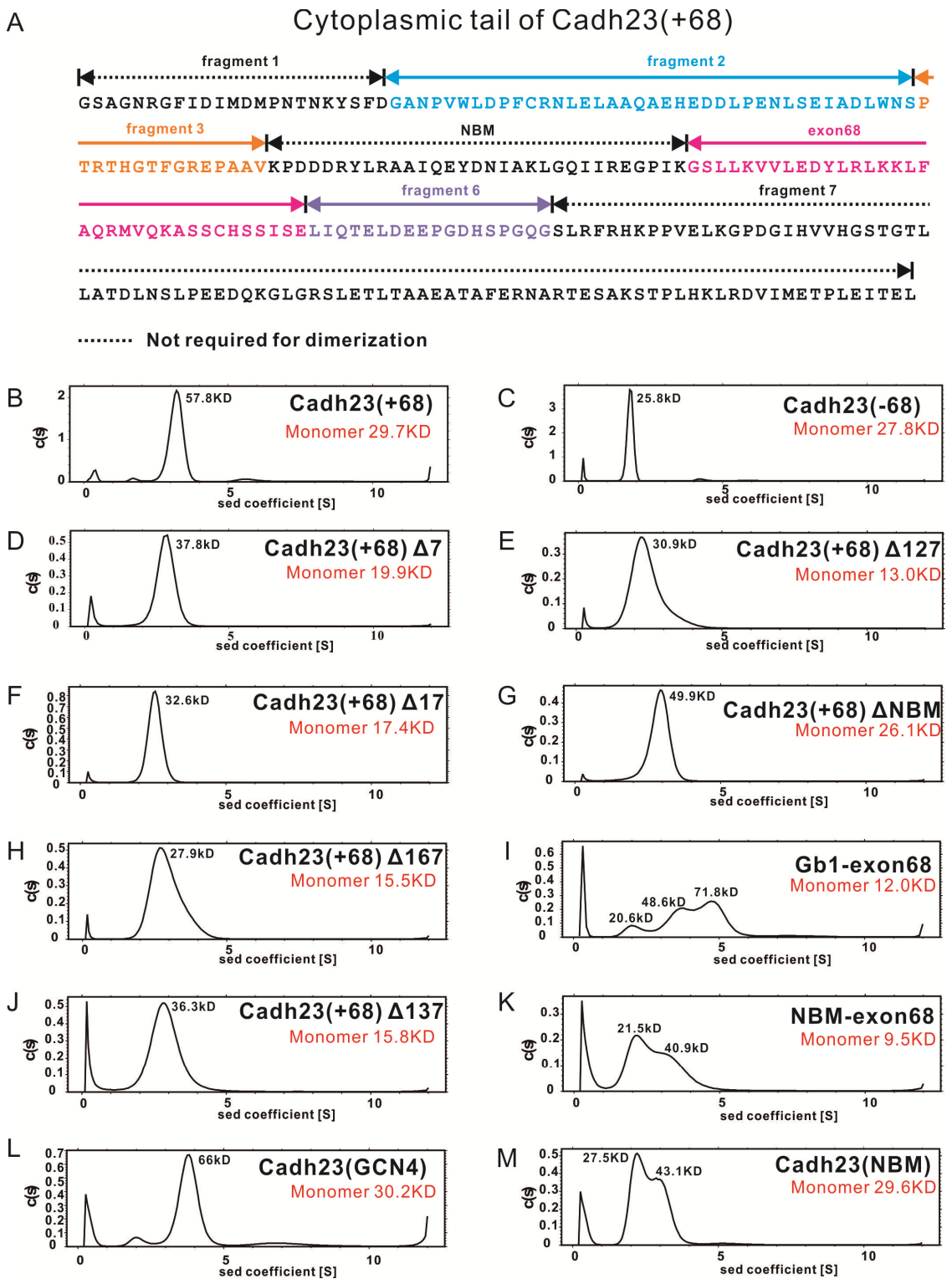
A
Cytoplasmic tail of Cadh23(+68)
fragment 1
fragment 2
GSAGNRGFIDIMDMPNTNKYSFDGANPVWLDPFCRNLELAAQAEHEDDLPENLSEIADLWNSP
fragment 3
NBM
exon68
TRTHGTFGREPAAVKPDDDRYLRAAIQEYDNIAKLGQIIREGPIKGSLLKVVLEDYLRLKKLF
fragment 6
fragment 7
AQRMVQKASSCHSSISELIQTELDEEPGDHSPGQGSLRFRHKPPVELKGPDGIHVVHGSTGTL
LATDLNSLPEEDQKGLGRSLETLTAAEATAFERNARTESAKSTPLHKLRDVIMETPLEITEL
Not required for dimerization
B
57.8KD
Cadh23(+68)
Monomer 29.7KD
C
25.8kD
Cadh23(-68)
Monomer 27.8KD
D
37.8kD
Cadh23(+68) Δ7
Monomer 19.9KD
E
30.9kD
Cadh23(+68) Δ127
Monomer 13.0KD
F
32.6kD
Cadh23(+68) Δ17
Monomer 17.4KD
G
49.9KD
Cadh23(+68) ΔNBM
Monomer 26.1KD
H
27.9kD
Cadh23(+68) Δ167
Monomer 15.5KD
I
20.6kD
48.6kD
71.8kD
Gb1-exon68
Monomer 12.0KD
J
36.3kD
Cadh23(+68) Δ137
Monomer 15.8KD
K
21.5kD
40.9kD
NBM-exon68
Monomer 9.5KD
L
66kD
Cadh23(GCN4)
Monomer 30.2KD
M
27.5KD
43.1KD
Cadh23(NBM)
Monomer 29.6KD
c(s)
sed coefficient [S]

Supplemental Figure S3. Analytical ultracentrifugation-based molecular weight measurements of various cadherin23 cytoplasmic tail fragments. *A,* The cytoplasmic tail of cadherin23(+68) is divided into 7 fragments, and the different fragments are applied to analytical ultracentrifugation for molecular mass determination. *B-K*, Sedimentation velocity profiles of different cadherin23 fragments showing fragment 2, fragment 3, exon68 and fragment 6 are all required for efficient cadherin23 tail dimerization. The calculated molecular weights of different fragments are shown in black, and the theoretical weights are in red. *L-M,* Sedimentation velocity profiles of cadherin23(GCN4) and cadherin23(NBM), showing that the replacement of exon68 encoded sequence with GCN4 dimer can also lead to efficient dimerization of cadherin23. In contrast, the replacement of exon68 with NBM significantly compromised the dimerization capacity of cadherin23.

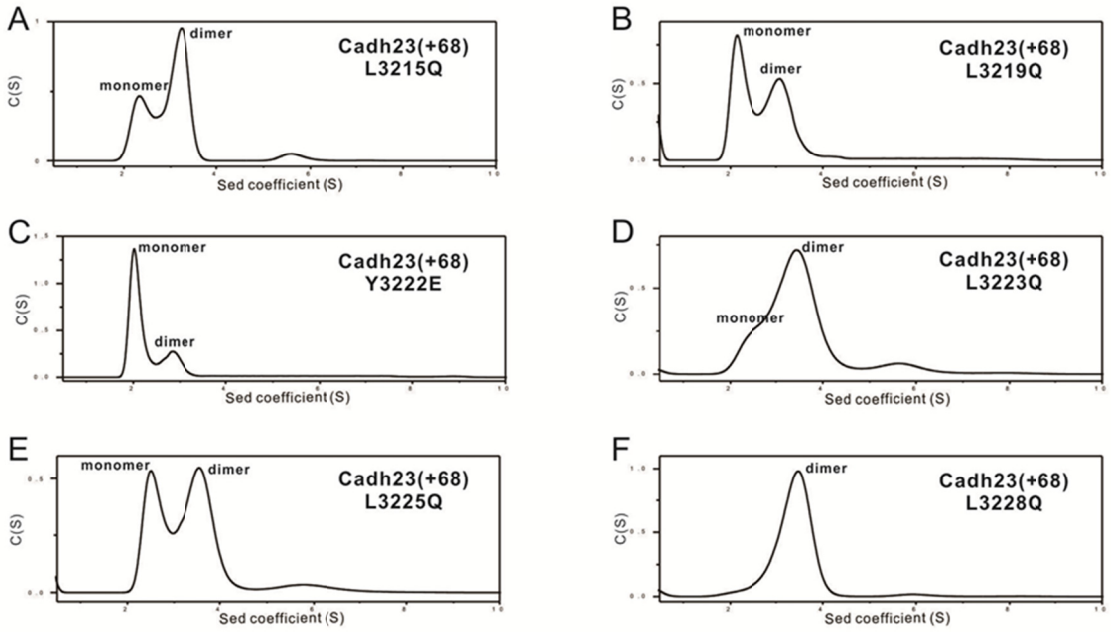

Supplemental Figure S4. Analytical ultracentrifugation-based identification of crucial residues within the exon68 encoded sequence required for the dimerization of cadherin23 cytoplasmic tail. Sedimentation velocity profiles of the cadherin23(+68) cytoplasmic tail with different mutations within the exon68 encoded sequence showing that individual substitution of Leu3215 (*A*), Leu3219 (*B*), Leu3223 (*D*), Leu3225 (*E*) with Gln, and Tyr3222 (*C*) with Glu all weakened the dimer formation. In contrast, substitution of Leu3228 with Gln (*F*) had little effect on the dimer formation of cadherin23 cytoplasmic tail. It is noted that Leu3215, Leu3219 and Tyr3222 are also essential for the exon68 peptide to bind to NTD (see Supplemental Figure S2).